Chapter 2

Intrinsic Dynamics of an Excitatory-Inhibitory Neural Pair

A pair of an excitatory and an inhibitory neurons, coupled to each other and evolving in discrete time intervals, is one of the simplest systems capable of showing chaotic behavior. This has guided the choice of this system for extensive study in this thesis. The present chapter examines the discrete-time dynamics of such coupled neuron pairs with four different types of nonlinear activation functions. The complex dynamical behavior of the system is generic for the different types of activation functions considered here. Features specific to each of the functions, were also observed. For example, in the case of piecewise linear functions, border-collision bifurcations and multifractal fragmentation of the phase space occurred for a range of parameter values. Anti-symmetric activation functions show a transition from symmetry-broken chaos (with multiple coexisting but disconnected attractors) to symmetric chaos (when only a single chaotic attractor exists). The model can be extended to a larger number of neurons, under certain restrictive assumptions, which makes the resultant network dynamics effectively one-dimensional. Possible applications of the network for information processing have been outlined. These include using the network for auto-association, pattern classification, nonlinear function approximation and periodic sequence generation.

The rest of the chapter is organized as follows. The basic features of the neural model used is described in section 1, along with the biological motivation for such a model. The next section is devoted to analyzing the dynamics of a pair of excitatory and inhibitory neurons, with self- and inter-connections. Two specific types of activation functions are chosen for detailed investigation, with either (*i*) asymmetric, piecewise linear, or, (*ii*) anti-symmetric, sigmoid characteristics. This simple system shows a wide range of behavior including periodic cycles and chaos. In section 3, we discuss the effect of introducing a non-zero threshold (or "bias"), which is equivalent (in the present model) to subjecting the system to a constant external input. Section 4 extends the model to larger networks under certain restrictive conditions. This is followed by a discussion of the possible application of the model to various information processing tasks, such as associative memory and nonlinear function approximation. The rich dynamics of the system allows it to respond to specific inputs with periodic or aperiodic responses (in contrast with convergent networks, which give time-independent constant output) and also to act as a *central pattern generator.* We conclude with a short discussion on possible ramifications of the model.

2.1 Single 'neuron' behavior

Let u_n denote the activation state of a model neuron at the $n-$th time interval. If $u_n = 1$, the neuron is considered to be active (firing), and if $u_n = 0$, it is quiescent. Then, if v_n is the input to the neuron at the nth instant and θ be the threshold, the discrete-time neural dynamics is described by the equation

$$u_n = \mathcal{F}(v_n \ - \theta), \tag{2.1}$$

assuming there to be no effects of delay. The input v_n is the weighted sum of the activation states of all other neurons, at the $(n-1)$-th instant, that are connected to the neuron under consideration, together with external stimulus (if any). The form of $\mathcal{F}$ is decided by the input-output behavior of the neuron. Usually, it is taken to be the *Heaviside step function*, i.e.,

$$\begin{aligned} \mathcal{F}(z) &= 1, \text{ if } z > \theta, \\ &= 0, \text{ otherwise,} \end{aligned} \tag{2.2}$$

where θ is known as the *threshold.*

If the *mean firing rate*, i.e., the activation state averaged over a time interval, is taken as the dynamical variable, then a continuous state space is available to the system. If X_n be the mean firing rate at the $n-$th time interval, then

$$X_{n+1} \ = \ F_\mu(\Sigma_j W_j X_n^j + I_n - \theta_n). \tag{2.3}$$

Here, F is known as the *activation function* and μ is the parameter associated with it. The first term of the argument represents the weighted sum of inputs from all neurons connected with the one under study. W_j is the synaptic weightage for the connection to the jth neuron. I_n and θ_n represent the external stimulus and threshold respectively, at the nth instant.

Considering the detailed biology of a neuron, there are two transforms occurring at the threshold element. At the input end, the impulse frequency coded information is transformed into the amplitude modulation of the neural current. For single neurons, this pulse-wave transfer function is linear over a small region, with nonlinear saturation at both extremities. At the output end, the current amplitude is converted back to impulse frequency. The wave-pulse transfer-function for single neurons is zero below a threshold, then rises linearly upto a maximum value. Beyond this maximum, the output falls to zero due to "cathodal block". These relations are time-dependent. For example, the slope of the wave-pulse transfer function decreases with time when subjected to sustained activation - this is known as "adaptation" [53].

The net transformation of a input by a neuron is therefore given by the combined action of the two transfer-functions. Let us approximate the nonlinear pulse-wave transfer function F_1 with a piecewise linear function, such that

$$\begin{aligned} F_1(z) &= -c, \text{ if } z < -c/m, \\ &= m\, z, \text{ if } -c/m \le z \le 1/m, \\ &= 1, \text{ if } z > 1/m. \end{aligned} \tag{2.4}$$

The wave-pulse transfer function F_2 is represented as

$$\begin{aligned} F_2(z) &= 0, \text{ if } z < \theta, \\ &= m' \,(z-\theta), \text{ if } \theta \le z \le \theta + (1/m'), \\ &= 0, \text{ if } z > \theta + (1/m'), \end{aligned} \tag{2.5}$$

where m, m' are the slopes of F_1, F_2 respectively, c is the inhibitory saturation value and θ represents a threshold value.

It is easily seen that the combined effect of the two gives rise to the resultant transfer function, G, defined as

$$\begin{aligned} G(z) &= 0, \text{ if } z < \theta, \\ &= m\, m' \,(z-\theta), \text{ if } \theta \le z \le \theta + (1/m), \\ &= m' \,(1-\theta), \text{ if } \theta + (1/m) < z \le \theta + (1/m'), \\ &= 0, \text{ if } z > \theta + (1/m'). \end{aligned} \tag{2.6}$$

In the present work we will assume that $m' \,(1-\theta) << \theta + (1/m')$. This condition ensures that the operating region of the neuron does not go into the "cathodal block" zone. This allows us to work with the following simplified, piecewise linear neural activation function (upon rescaling) throughout the rest of the thesis:

$$\begin{aligned} F_a(z) &= 0, \text{ if } z < \theta, \\ &= a\,(z-\theta), \text{ if } \theta \le z \le \theta + (1/a), \\ &= 1, \text{ if } z > \theta + (1/a), \end{aligned} \tag{2.7}$$

where a (> 0) is called the *gain parameter* of the function (Figure 2.1 (a)). Note that, this activation function is *asymmetric* as it corresponds to an input-output mapping of the form $(-\infty, \infty) \rightarrow [0, 1]$. For infinite gain ($a \rightarrow \infty$), the activation function reverts to the hard-limiting Heaviside step function.

The piecewise linear nature of the model neuron used, not only makes detailed theoretical analysis possible, but also enables an intuitive understanding of the dynamics, at least for a small number of connected elements. This makes it easier to extrapolate to larger networks and suggest possible applications. The proposed model is also particularly suitable for hardware implementation using operational amplifiers (owing to their piecewise linear characteristics).

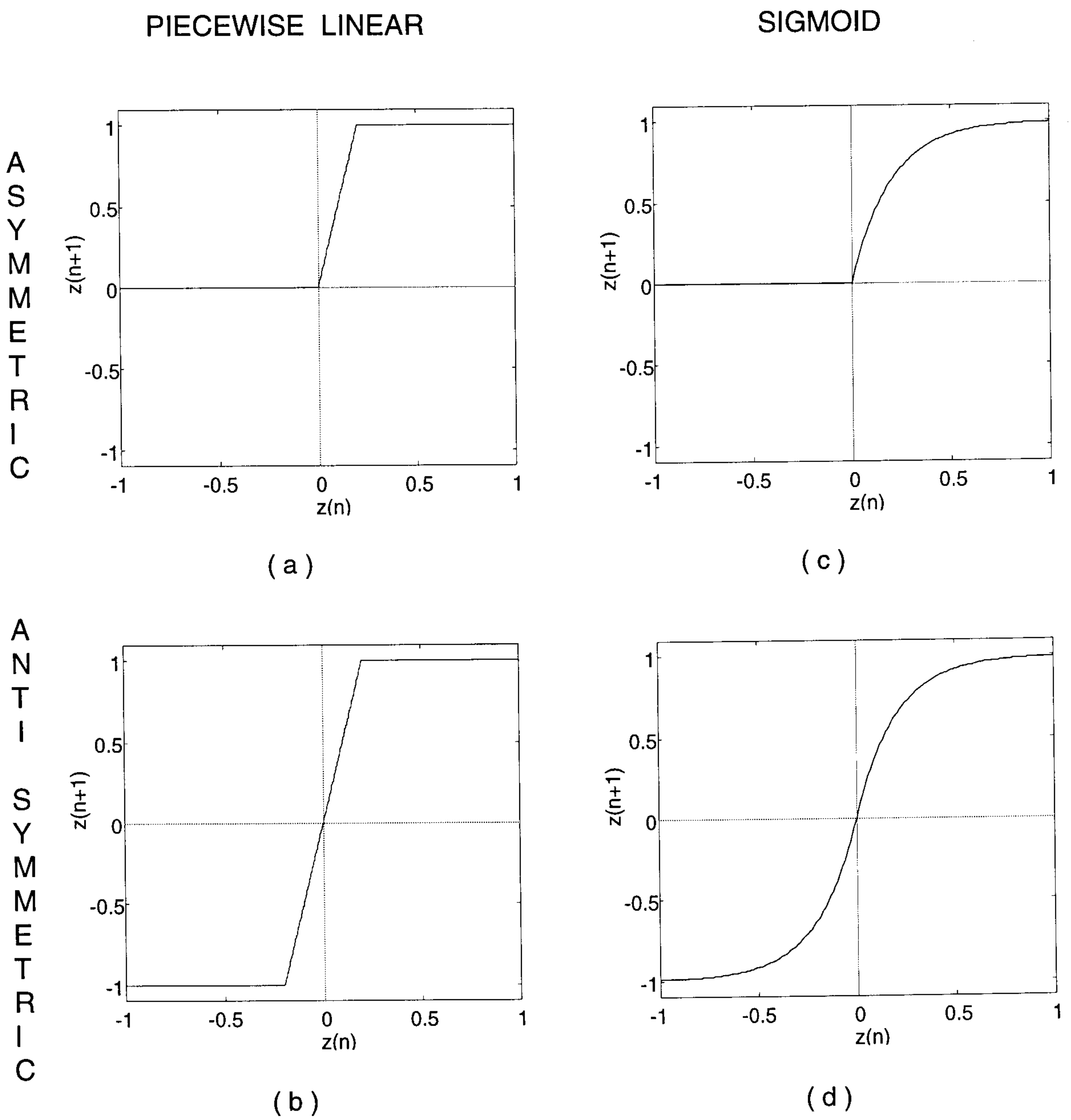

Figure 2.1: The different activation functions (F_a) for a single neuron (gain parameter, $a = 5$) having (a) asymmetric, piecewise linear, (b) anti-symmetric, piecewise linear, (c) asymmetric, sigmoid, and (d) anti-symmetric, sigmoid characteristics.

On translation and scaling, we obtain an *antisymmetric* form of this activation function, viz.

$$\begin{aligned} F_a(z) &= -1, \text{ if } z < \theta - (1/a), \\ &= a\,(z-\theta), \text{ if } \theta - (1/a) \leq z \leq \theta + (1/a), \\ &= 1, \text{ if } z > \theta + (1/a), \end{aligned} \tag{2.8}$$

so that the input-output mapping is now of the form $(-\infty, \infty) \to [-1, 1]$ (Fig. 2.1 (b)).

Although, in the present study, the gain parameter, a, of the transfer function is considered constant, in general it will be a time-varying function of the activation state, decreasing under constant external stimulation until the neuron goes into a quiescent state. The threshold θ is also a dynamic parameter, changing as a result of external stimulation. We have also assumed that the neuron state at the nth instant is a function of the state value at the previous instant only. Introducing delay effects into the model, such that,

$$X_{n+1} = F(X_n, X_{n-1}, \ldots, X_{n-\tau}),$$

might lead to novel behavior. This is discussed briefly in the concluding section.

If we now consider neural populations, instead of single neurons, then sigmoidal activation functions of the form

$$\begin{aligned} F_a(z) &= 1 - e^{-az}, \text{ if } z > 0, \\ &= 0, \text{ otherwise}, \end{aligned} \tag{2.9}$$

are the appropriate choice (Fig. 2.1 (c)). Note that, the output of a neural population is not a train of pulses (as in single neuron) but a continuous pulse density. By varying a, transfer functions with different slopes are obtained. In the neurobiological situation, the slope is both state-dependent (e.g., it increases with the behavioral arousal of a subject) and input-dependent (increasing with sensory excitation). In this work, we have taken a to be constant.

As in the piecewise linear case, here also we can define an antisymmetric form of the activation function (Fig. 2.1 (d)) as follows:

$$\begin{aligned} F_a(z) &= 1 - e^{-az}, \text{ if } z > 0, \\ &= -(1 - e^{az}), \text{ otherwise}. \end{aligned} \tag{2.10}$$

Note that for all the activation functions defined so far (i.e., Eqns. (2.7), (2.8), (2.9) and (2.10)), the following common features hold:

- $F(0) = 0$, i.e., 0 is a 'fixed-point' of the function, and
- the functions saturate at an output value, arbitrarily set to unity.

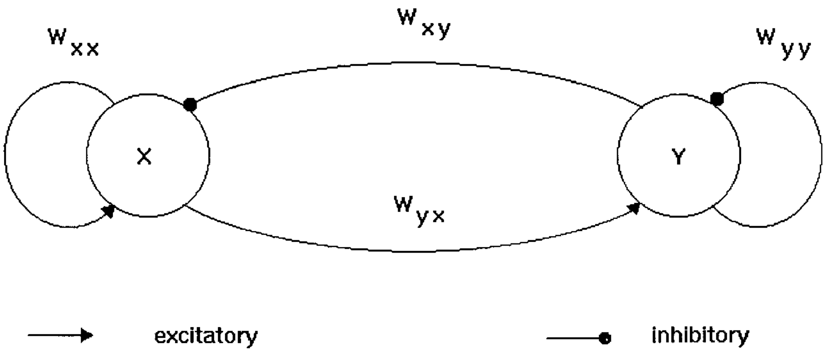

Figure 2.2: The pair of excitatory (x) and inhibitory (y) neurons. The arrows and circles represent excitatory and inhibitory synapses, respectively.

2.2 Excitatory-inhibitory pair dynamics

Having established the response properties of single neurons, we can now study the dynamics when they are connected. It is observed that, even connecting only an excitatory and an inhibitory neuron with each other leads to a rich variety of behavior, including high period oscillations and chaos. The continuous-time dynamics of pairwise connected excitatory-inhibitory neural populations (with sigmoidal nonlinearity) have been studied before [204]. However, an autonomous two-dimensional system (i.e., one containing no explicitly time-dependent term), evolving continuously in time, cannot exhibit chaotic phenomena, by the Poincare-Bendixson theorem [188]. In the present case, the resultant system is updated in discrete-time intervals and the dynamics is governed by one of the nonlinear activation functions defined in the previous section. This makes chaotic behavior possible in the proposed neural network model.

If X and Y be the mean firing rates of the excitatory and inhibitory neurons, respectively, then their time evolution is given by the coupled difference equations:

$$\begin{aligned} X_{n+1} &= F_a(W_{xx}X_n - W_{xy}Y_n), \qquad (2.11) \\ Y_{n+1} &= F_b(W_{yx}X_n - W_{yy}Y_n). \end{aligned}$$

The network connections are shown in Fig. 2.2. The W_{xy} and W_{yx} terms represent the synaptic weights of coupling between the excitatory and inhibitory elements, while W_{xx} and W_{yy} represent self-feedback connection weights. Although a neuron coupling to itself is biologically implausible, such connections are commonly used in neural network models to compensate for the omission of explicit terms for synaptic and dendritic cable delays [53].

Without loss of generality, the connection weightages W_{xx} and W_{yx} can be absorbed into the gain parameters a and b and the correspondingly rescaled remaining connection weightages, W_{xy} and W_{yy}, are labeled k and k' respectively. For convenience,

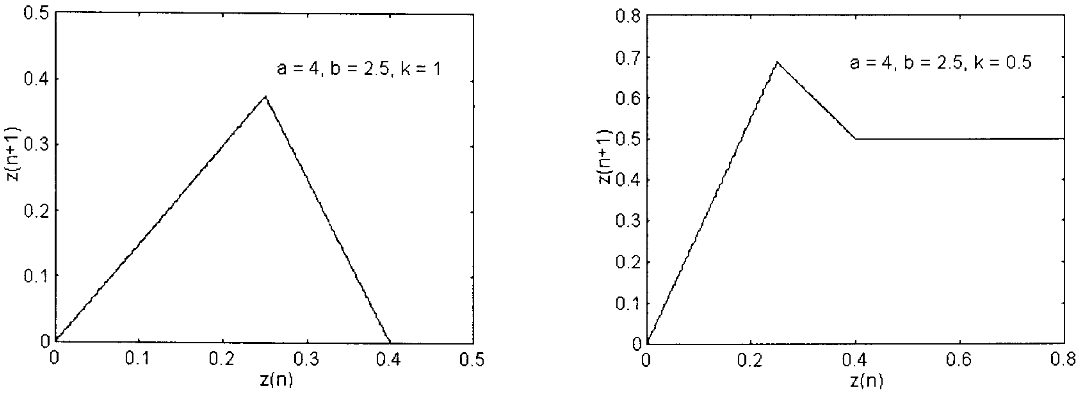

(a) (b)

Figure 2.3: The one-dimensional map representing neural pair dynamics with asymmetric, piecewise linear F for (a) $k = k' = 1$ and (b) $k = k' \neq 1$.

a transformed set of variables, $Z_n = X_n - k\ Y_n$ and $Z'_n = X_n - k'\ Y_n$, is used. The dynamics is now given by

$$Z_{n+1} = F_a(Z_n) - k\ F_b(Z'_n), \tag{2.12}$$

$$Z'_{n+1} = F_a(Z_n) - k'\ F_b(Z'_n).$$

Note that, if $k = k'$, the two-dimensional dynamics is reduced effectively to that of an one-dimensional difference equation ("map"), simplifying the analysis. We shall now consider in detail the dynamics of the map, when F has either (i) asymmetric, piecewise linear nature, or (ii) anti-symmetric, sigmoid character.

2.2.1 Asymmetric, piecewise linear activation function

Chaotic activity has been previously observed in piecewise linear systems, for both continuous-time [157] as well as discrete-time evolution [132, 133] of the system. In the following investigation, we shall examine the cases: $(i) k = k' = 1$, $(ii) k = k' \neq 1$, and $(iii) k \neq k'$, in detail. Throughout the present section, the threshold, θ, will be taken as 0 (a non-zero value of θ introduces some new phenomena, which will be investigated in the next Section).

Case I: $k = k' = 1$

This represents the condition when the connection weights $W_{xy} = W_{xx}$ and $W_{yy} = W_{yx}$, $(a > b)$. The dynamics is that of an *asymmetric tent map* (Fig. 2.3 (a)):

$$\begin{aligned} Z_{n+1} &= (a\ -\ b)\ Z_n, \text{ if } 0 \leq Z_n \leq 1/a, \\ &= 1\ -\ bZ_n, \text{ if } 1/a < Z_n \leq 1/b, \\ &= 0, \text{ otherwise.} \end{aligned} \tag{2.13}$$

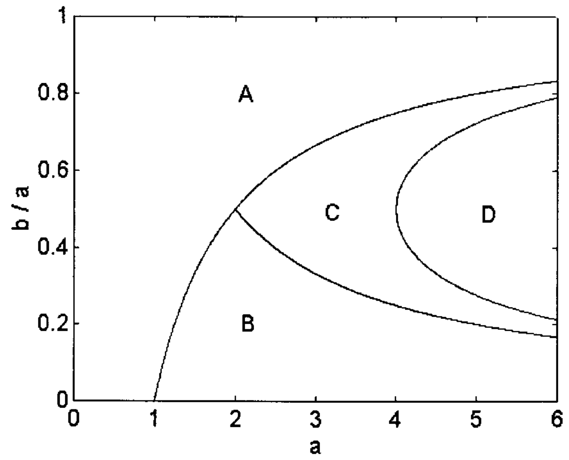

Figure 2.4: The activation gain a vs. (b/a) parameter space for $k = k' = 1$. Region A: $z^* = 0$ stable, B: $z^* = 1/(1+b)$ stable, C: chaos, D: coexistence of $z^* = 0$ and a fractal chaotic invariant set.

The fixed points of this system are, $Z_1^* = 0$ and $Z_2^* = 1/(1+b)$. Z_1^* is stable for $a - b < 1$, whereas Z_2^* exists only when $a - b > 1$, and is stable for $b < 1$. Beyond this, chaotic behavior is observed unless the maximum output value, i.e., $1 - (b/a)$, maps to $Z > 1/b$. The parameter space diagram is shown in Fig. 2.4. Along the line $b/a = 0.5$, we get the symmetric tent map scenario. So the Lyapunov exponent [1] along this curve grows as $\lambda = \log_e(b)$ for $0 < a < 4$. This is one of the two special cases where an analytical expression for λ can be obtained. The other instance is when the map's invariant probability distribution, $P(Z) = 1$. This occurs when

$$F\ (1/a) = 1 - (b/a) = 1/b. \tag{2.14}$$

Along the curve defined by the above relation, the Lyapunov exponent evolves with the parameter b/a according to

$$\lambda = -b/a\ \log_e(b/a) - (1 - (b/a))\log_e(1 - (b/a)). \tag{2.15}$$

In general, λ has to be obtained computationally. Fig. 2.5 shows λ plotted against b/a for $a = 4$, when the map is in the chaotic region. A sharp drop to zero is observed in both the terminal points, indicating sharp transition between chaotic and fixed-point behavior at $b/a = 0.25$ and 0.75. At $b/a = 0.5$, the entire interval $[0, 1/b]$ is uniformly visited by the chaotic trajectory ($P(Z) = 1$). This corresponds to "fully-developed chaos" in the symmetric tent map for which $\lambda = \log_e(2) \simeq 0.693$.

---

[1] Lyapunov exponent (λ) is a quantitative indicator of chaotic behavior. It is defined for a one-dimensional mapping F as:

$$\lambda = \mathrm{Lim}_{N\to\infty}\frac{1}{N}\log_e|\sum_{i=0}^{N-1}\frac{dF}{dx}|_{x=x_i}.$$

Chaotic behavior is indicated by a positive value of λ.

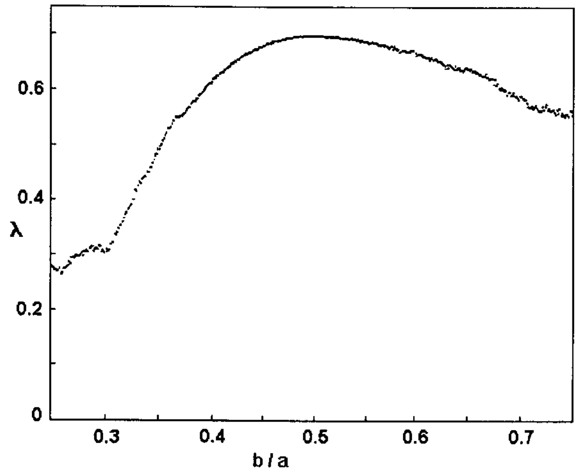

Figure 2.5: Lyapunov exponent of the chaotic dynamics for $k = k' = 1$ and $a = 4.0$. At $b/a = 0.5$, the entire interval $[0, 1/b]$ is uniformly visited.

When $F(1/a) > 1/b$, the interval $[0, 1/b]$ is divided into a chaotic region of measure zero, defined on a non-uniform Cantor set (in general) and an "escape set" which maps to $Z_1^* = 0$. This is because, for $Z \in (1/b(a-b), (b-1)/b^2)$, F(Z)=0. Any time an iterate of Z falls in this region, in the next iterate the trajectory will converge to Z_1^*. The points left invariant after one iteration, will be in the two intervals $[0, 1/b(a-b)]$ and $[(b-1)/b^2, 1]$. The phase space is thus fragmented into two invariant regions. After n iterations, there will be 2^n fragments of the chaotic invariant set, with $n!/r!(n-r)!$ $(r = 0, 1, \ldots, n)$ intervals of length $(a-b)^r(1-b)^{r-n}$. The fragmentation of the phase space, therefore, has a *multifractal* nature [123].

The presence of multiple length scales is due to the fact that the slope magnitude of the map is not constant throughout the interval $[0, 1/b]$. It is to be noted that, even for Z not belonging to the fractal invariant set, the trajectory might show long *chaotic transients* until at some iterate it maps to $Z^* = 0$. For $b/a = 0.5$, the map has a constant slope. As a result, the Cantor set is uniform, having exact geometrical self-similarity and a fractal dimension, $D = \log_e(2)/\log_e(b)$. So, the phase space of the coupled system has a fractal structure in this parameter region, i.e., where $1 - (b/a) > 1/b$.

Fig. 2.6 shows the bifurcation structure of the map for $a = 4$. For $b/a < 0.25$, the fixed point Z_2^* is stable. At $b/a = 0.25$ it becomes unstable, leading to bands of chaotic behavior. The chaotic bands collide with the unstable fixed point Z_2^* at $b/a \simeq 0.2985...$ and merge into a single chaotic band. This band-merging transition is an example of *crisis* [69] and has been studied in detail for the symmetric tent map [206]. The b-value at which the band-merging occurs for a given value of a, can be obtained analytically by solving the quartic equation:

$$b^4 + (1 - 2a)b^3 + (a^2 - a)b^2 + ab + (a - a^2) = 0. \tag{2.16}$$

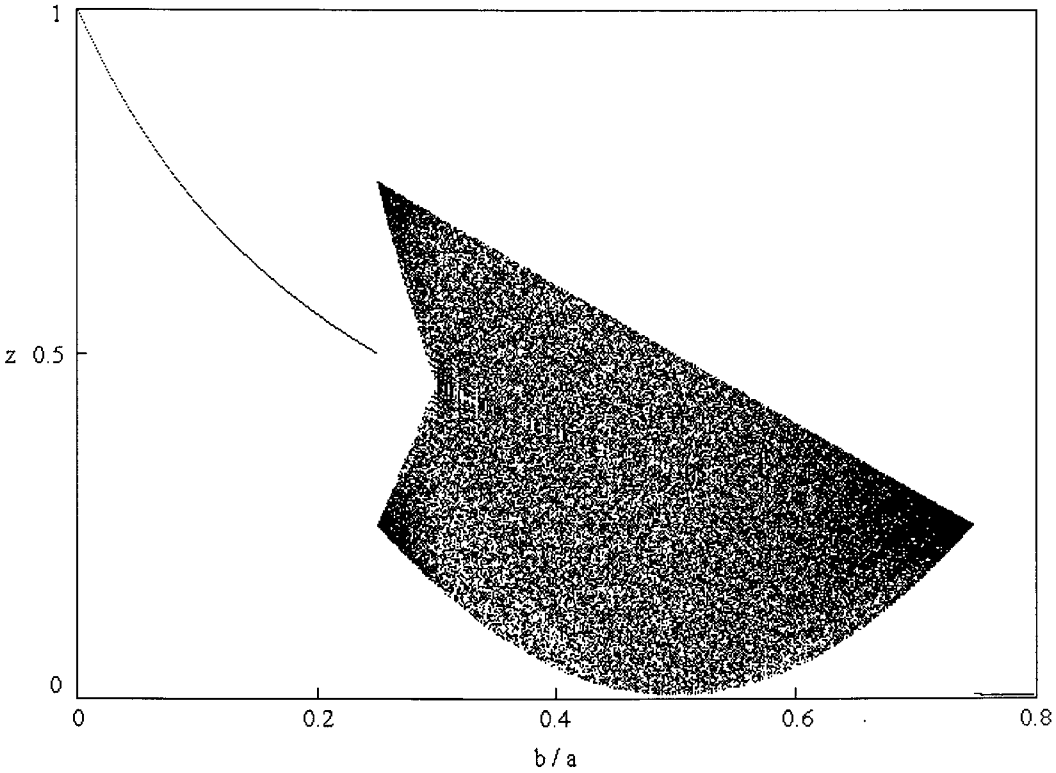

Figure 2.6: Bifurcation diagram for $k = k' = 1$ at $a = 4.0$.

For $2 < a < 2.5$, all the roots are complex, implying that band-merging does not occur over this range of a-values.

Uniform chaotic behavior occurs at $b/a = 0.5$ (the entire interval [0,1/b] is uniformly visited by the chaotic trajectory). The chaotic band collides with the unstable Z_2^* again at $b/a = 0.75$. This boundary crisis destroys chaos and stabilizes the fixed point $Z_1^* = 0$.

Case II: $k = k' \neq 1$

This represents the condition when the connection weightages are such that, $W_{xy}/W_{xx} = W_{yy}/W_{yx} = k$, $(a > b)$. The dynamics is given by the following map (Fig. 2.3 (b))

$$\begin{aligned} Z_{n+1} &= (a - kb)\, Z_n, \text{ if } 0 \leq Z_n \leq 1/a, \\ &= 1 - kbZ_n, \text{ if } 1/a < Z_n \leq 1/b, \\ &= 1 - k, \text{ otherwise.} \end{aligned} \tag{2.17}$$

The key difference with the earlier case is that, now, the dynamics supports superstable period-m orbits $(m \geq 2)$. This is a result of the existence of a region of zero slope $(Z > 1/b)$ giving a non-zero output. There are two fixed points of the map, $Z_1^* = 0$ (as before), and,

$$\begin{aligned} Z_2^* &= 1 - k, \text{ if } 0 < k < 1 - (1/b), \text{ or,} \\ &= 1/(1 + kb), \text{ if } (a-1)/b > k > 1 - (1/b). \end{aligned}$$

$Z_2^* = 1 - k$, if it exists, is superstable, as the local slope is zero. On the other hand, $Z_2^* = 1/(1 + kb)$ is stable, only if $bk < 1$. If the fixed points are unstable, but iterates of Z fall in the region $Z > 1/b$, superstable periodic cycles occur. The fixed point, $Z_1^* = 0$, becomes stable when $(a - bk) < 1$. Chaotic behavior occurs if none of the fixed points are stable, and no iterate of Z falls in the region $Z > 1/b$. The (b/a) vs. k parameter space diagram in Fig. 2.7 (for $a = 4$) shows the different dynamical regimes that are observed.

The bifurcation diagram for $a = 4, b = 2$ (Fig. 2.8) shows how the dynamics changes with k. For $0 \leq k < 0.5$, $Z_2^* = 1 - k$, is the stable fixed point. At $k = 0.5$, Z_2^* becomes unstable, giving rise to a superstable period-2 cycle. A periodic regime is now observed, which was absent in the previous case. The periodic orbits initially follow a *period-doubling* sequence until a period-32 $(= 2 \times 2^4)$ orbit gives rise to a period-48 $(= 3 \times 2^4)$ one. This occurs as a result of a border-collision bifurcation by which "period-2 to period-3" bifurcations have been seen to occur [132, 133]. In the above instance, each of the sixteen period-2 orbits give rise to a period-3 orbit. The structure of the superstable periodic orbits is quite complex. The length of the cycles is plotted against k in Fig. 2.9. The remarkable self-similar structure of the intervals is to be noted. Numerical studies indicate that cycles of all periods exist having the following ordering: between any superstable period-m and period-$(m+1)$ cycle, there exists an interval of k for which a period-$(m + 2)$ orbit is superstable. At $k = 1.0$ all periodic orbits become unstable, leading to onset of chaos. The chaotic behavior persists till $k = 1.5$, when $Z_1^* = 0$ becomes stable. The sequence of the periodic cycles

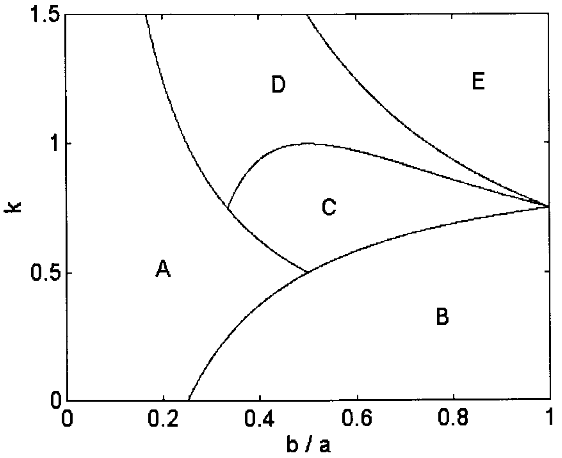

Figure 2.7: The (b/a) vs. k parameter space for $k = k' \neq 1$ at $a = 4.0$. Region A: $z^* = 1/(1 + kb)$ stable, B: $z^* = 1 - k$ stable, C: superstable periodic cycles, D: chaos, E: $z^* = 0$ stable.

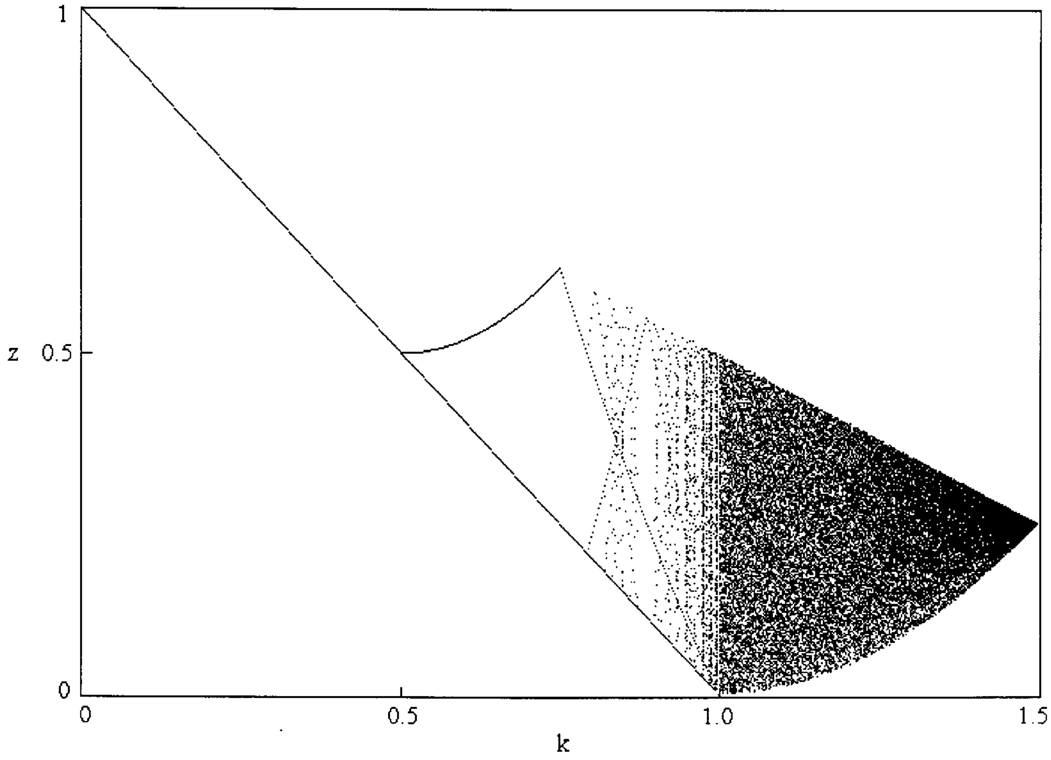

Figure 2.8: Bifurcation diagram for $k = k' \neq 1$ at $a = 4.0, b = 2.0$.

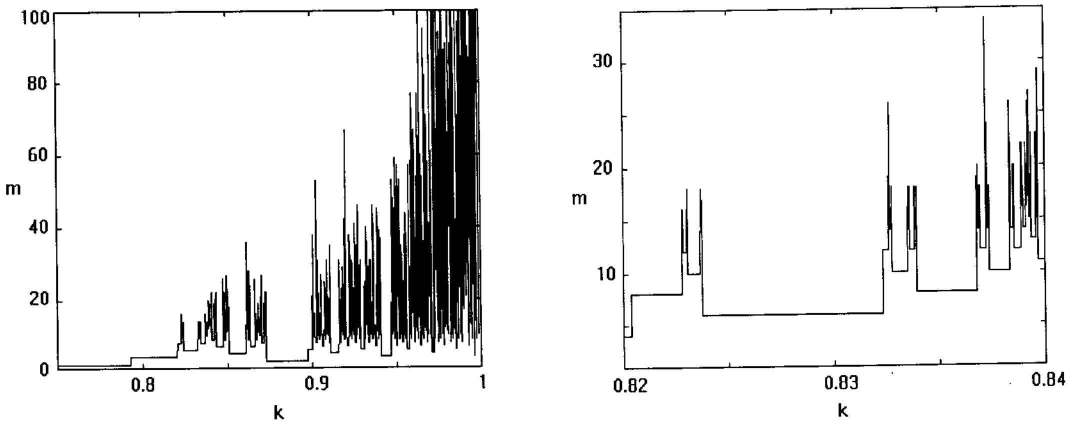

(a) (b)

Figure 2.9: Length of superstable periodic cycles, m, of the excitatory-inhibitory neural pair ($a = 4$, $b = 2$) for (a) $0.75 \leq \mathrm{k} < 1$, and (b) $0.82 \leq \mathrm{k} < 0.84$. Note the self-similar structure of the intervals.

is remarkably similar to that seen in the case of unidirectional, adaptive dynamics on a lattice of chaotic maps [165].

Case III: $k \neq k'$

This corresponds to the condition when all the connection weights are different. The dynamics is irreducible to 1-dimension. We need to consider only the positive (Z, Z') region, as otherwise, $(0,0)$ is the stable fixed point. In the non-zero region, different dynamical behavior may occur depending on the region where the fixed point occurs and on its stability. One of the fixed points is $(Z, Z') = (0,0)$, whose stability is determined by obtaining the eigenvalues of the corresponding Jacobian,

$$\mathbf{J} = \begin{vmatrix} a & -kb \\ a & -k'b \end{vmatrix} .$$

Evaluating the above matrix, gives the following condition

$$-2 < (a - k'b) \pm [(a - k'b)^2 - 4ab(k - k')]^{1/2} < 2, \tag{2.18}$$

for stability of the fixed point.

The other fixed point may occur in any one of the four following regions of the (Z, Z')-space:

Region I: $0 < Z < 1/a$, $0 < Z' < 1/b$.
$(Z, Z') = (0,0)$ is the only fixed point.

Region II: $0 < Z < 1/a$, $Z' > 1/b$.
The fixed point is $(Z, Z') = (k/(a-1), (a(k-k') + k')/(a-1))$, which is stable if $-1 < a < 1$.

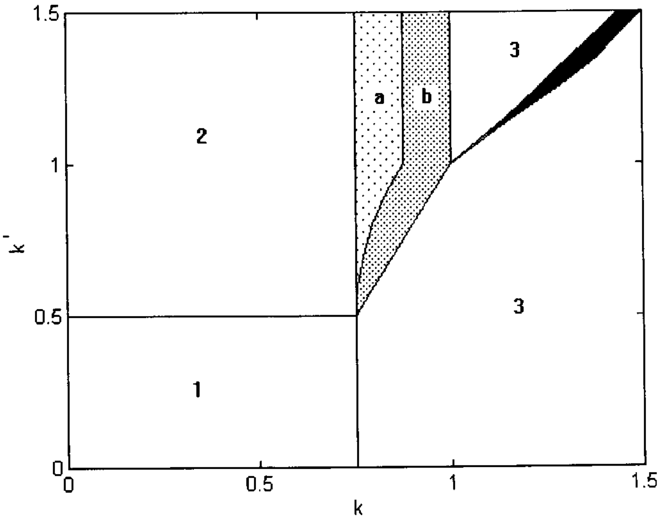

Figure 2.10: The (k, k') parameter space for $a = 4.0$ and $b = 2.0$. Region 1: $x^*=1$, $y^*=1$ stable, 2: $x^*=1$, y has period-2 cycles, 3: $x^*=0$, $y^*=0$ stable, a: Both x and y have period-2 cycles, b: x and y show period-m cycles ($m>2$). Fully chaotic behavior occurs in the dark wedge-shaped region in 3. In addition, fractal intervals showing chaos occur in region b.

Region III: $Z > 1/a$, $0 < Z' < 1/b$.
The fixed point is $(Z, Z') = ((1 + b(k' - k))/(1 + bk'), 1/(1 + bk'))$, which is stable if $-1 < k'b < 1$.

Region IV: $Z > 1/a$, $Z' > 1/b$.
The fixed point is $(Z, Z') = (1 - k, 1 - k')$. This is a superstable root, as the local slope is zero under all conditions.

The abundance of tunable parameters in this case, makes detailed simulation study extremely difficult. However, some preliminary studies in the (k, k') parameter space (keeping the other parameters fixed) gives indication of dynamics similar to that seen in cases (*i*) and (*ii*). The (k, k') parameter space is shown in Fig. 2.10 for $a = 4$, $b = 2$. A variety of dynamical behaviors is observed - from fixed points to periodic cycles to chaos, as indicated by the different regions. In addition, there are regions exhibiting periodic behavior which have fractal intervals of chaotic activity embedded within them.

2.2.2 Anti-symmetric, sigmoid activation function

We will now look at the dynamics of the excitatory-inhibitory neural pair when the activation function F is of the form (2.10). If $k = k'$, the resultant dynamics is that of a one-dimensional bimodal map, whose phase space is disconnected into two halves for $k \leq 1$. We shall consider first the case when $k = k' = 1$, and then investigate the change in the behavior of the system when $k = k' \neq 1$.

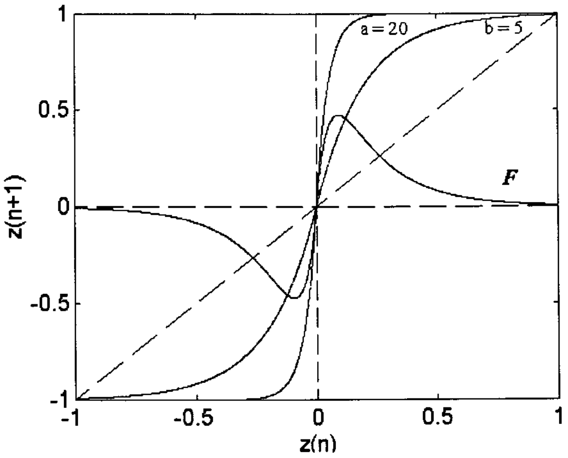

Figure 2.11: The sigmoid activation functions (F) for slopes, a=20 and b=5, and the resulting one-dimensional map.

For $k = 1$, the two halves of the phase space ($L : (-\infty, 0)$ and $R : [0, \infty)$ are not connected - i.e., a trajectory starting with an initial condition belonging to L, can never reach R in the course of time, and vice versa. The resulting dynamics is that of the following map:

$$\begin{aligned} Z_{n+1} &= \exp(-bZ_n) - \exp(-aZ_n), \text{ if } 0 \leq Z_n \leq \infty, \\ &= -\exp(bZ_n) + \exp(aZ_n), \text{ otherwise.} \end{aligned} \tag{2.19}$$

Fig. 2.11 shows the map, arising out of interaction between an excitatory neuron with slope, $a = 20$, and an inhibitory neuron with slope, $b = 5$. The bifurcation diagram of the map (Fig. 2.12), obtained by increasing the ratio b/a, keeping a fixed shows a transition from fixed point to periodic cycles and chaos, following a "period-doubling" route, an universal feature for an entire family of one-dimensional chaotic maps [188]. Fig. 2.13 shows a magnified image of the bifurcations, which clearly exhibits the successive doubling of the periodic cycles. The variation of a, keeping the ratio b/a fixed, also shows a transition to chaotic behavior, as is indicated in Fig. 2.14.

The map has 3 fixed points: $Z_1^* = 0$, Z_2^* and Z_3^* (by symmetry of the map, $Z_3^* = -Z_2^*$). The latter are the solutions of the transcendental equation $Z = \exp(-bZ) - \exp(-aZ)$. The fixed point Z_1^* is stable if the local slope ($\simeq (a - b)$) is less than 1. For $a > \frac{1}{1-\mu}$ (where, $\mu = \frac{b}{a}$), this condition no longer holds and Z_1^* loses stability while Z_2^* becomes stable by a transcritical bifurcation. On further increase of a, this fixed point also loses stability (by flip bifurcation) with the local slope becoming less than -1, and a 2-period cycle become stable. Increasing a further leads to cycles of higher and higher periods becoming stable, ultimately leading to totally aperiodic behavior.

The chaotic behavior can be quantified, as in the case of the piecewise linear function,

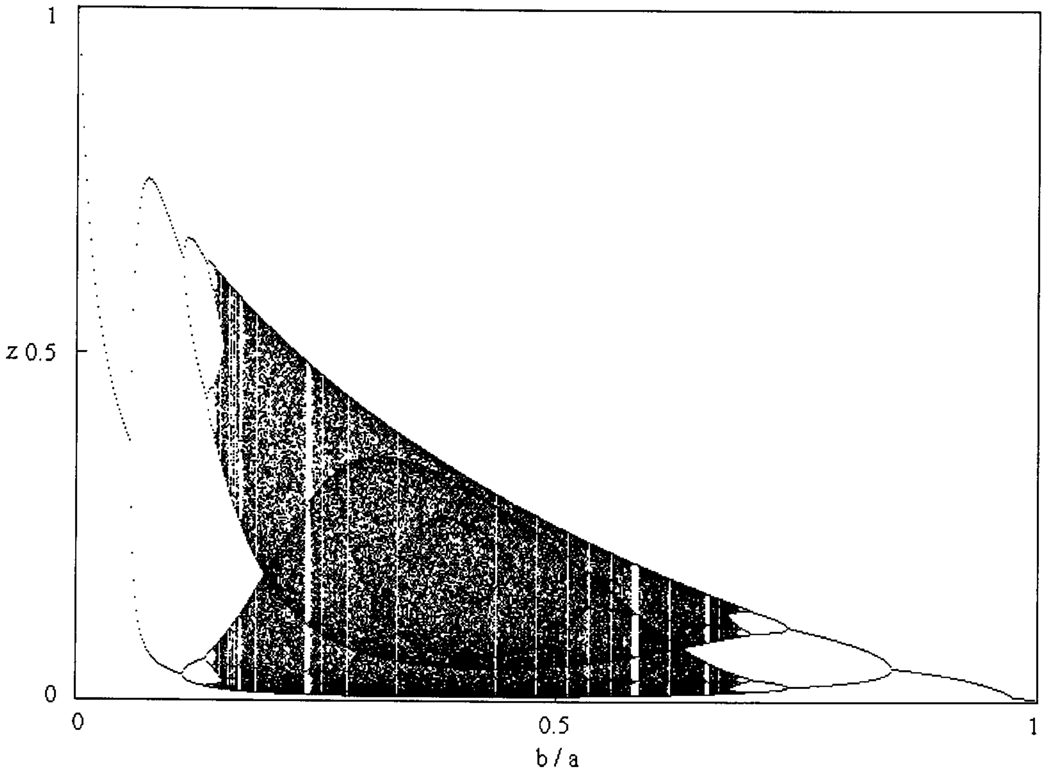

Figure 2.12: Bifurcation diagram of the map representing excitatory-inhibitory pair dynamics with sigmoid F for a=50.

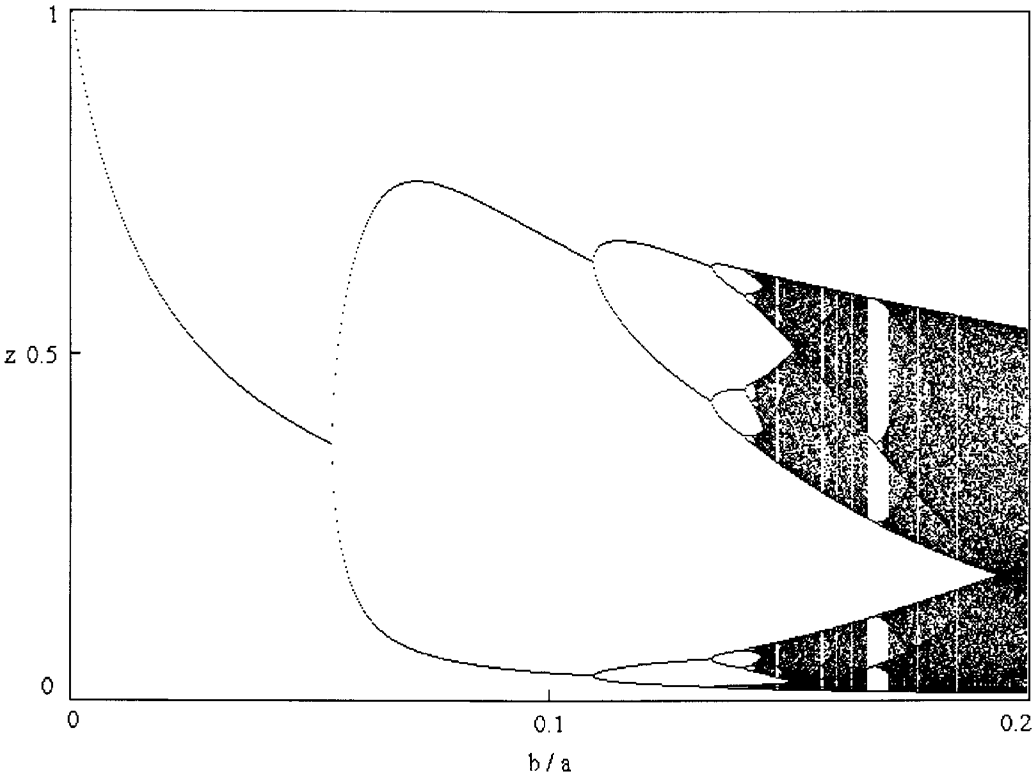

Figure 2.13: Magnified view of the preceding bifurcation diagram, over the interval $0 \leq b/a \leq 0.2$ (a=50).

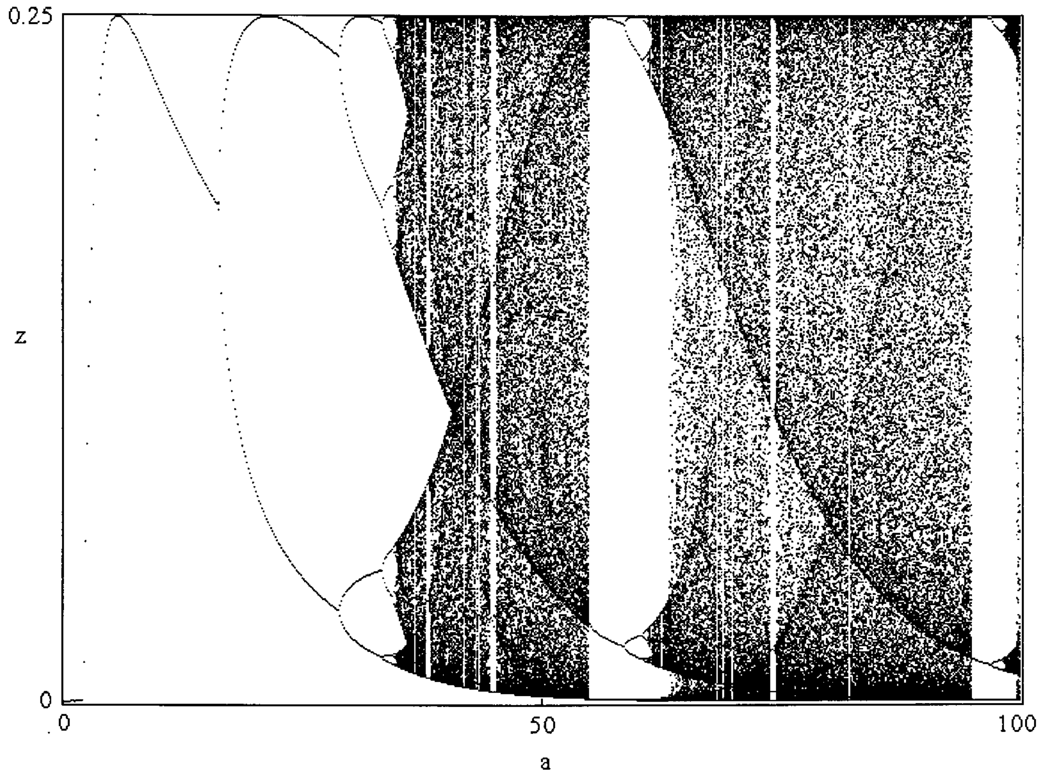

Figure 2.14: Bifurcation diagram of the map representing excitatory-inhibitory pair dynamics with sigmoid F for b/a=0.5.

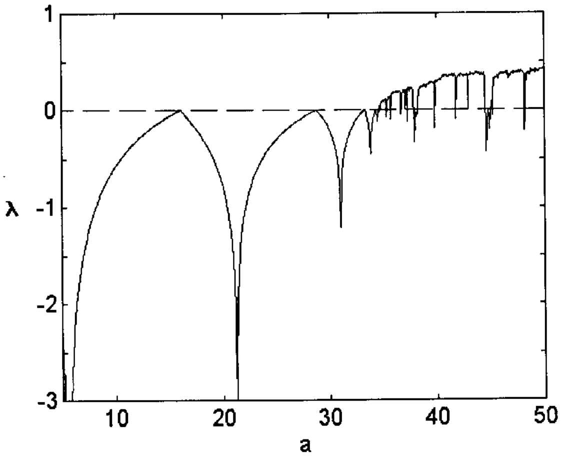

Figure 2.15: Lyapunov exponent (λ) plotted against a for $b/a = 0.5$.

by the Lyapunov exponent (λ). Fig. 2.15 shows the variation of λ with a ($b/a = 0.5$) and Fig. 2.16 exhibits the chaotic and non-chaotic regions on the basis of the sign of λ, with regions having $\lambda < 0$ (i.e., non-chaotic) indicated by black. Notice the "garlands" of periodic windows within the chaotic region. The isolated points of periodic behavior, interspersed throughout the chaotic region, are remnants of periodic windows too fine to be resolved at the present scale.

We shall now consider the case when $k = k' \neq 1$. Figs. 2.17 and 2.18 show the bifurcation diagrams at $a = 50$ and $b/a = 0.5$ over the intervals, ($0 \leq k \leq 1.5$) and ($0.99 \leq k \leq 1.03$), respectively. As k decreases from 1, the flatter end of the map rises, so that, very soon the local slope of the fixed point, Z_2^* (or, equivalently, Z_3^*), becomes greater than -1, making it stable. This is indicated by the long interval of non-chaotic behavior for $0 \leq k < 0.9$. When k increases from 1, the two disjoint chaotic attractors are dynamically connected - so that a transition from symmetry-broken chaos to symmetric chaos is observed. On further increase of k, chaos again gives rise to periodic, and finally, fixed point behavior.

2.3 Effect of threshold / bias

In the previous section, we have looked at the autonomous dynamics of the excitatory-inhibitory neural pair - i.e., in the absence of any external input. We had also assumed the threshold θ to be zero. We shall now look at the effect of both of these variables on the system variables. One of the simplifying features of the type of activation functions we have chosen is that introducing a threshold of magnitude θ is equivalent to subjecting the system to a constant external input of amplitude $|\theta|$. This is evident if we look at eqn. 2.12 for the case $k = k' = 1$, in the presence of

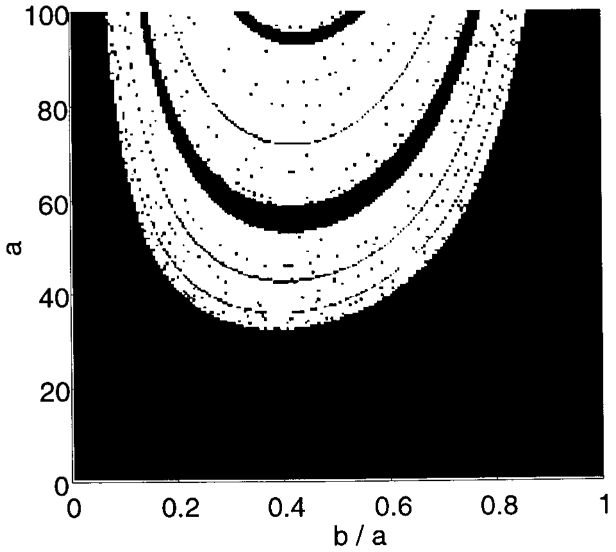

Figure 2.16: Stability diagram in the a vs (b/a) parameter space with ordered behavior indicated by black and chaotic behavior indicated by white.

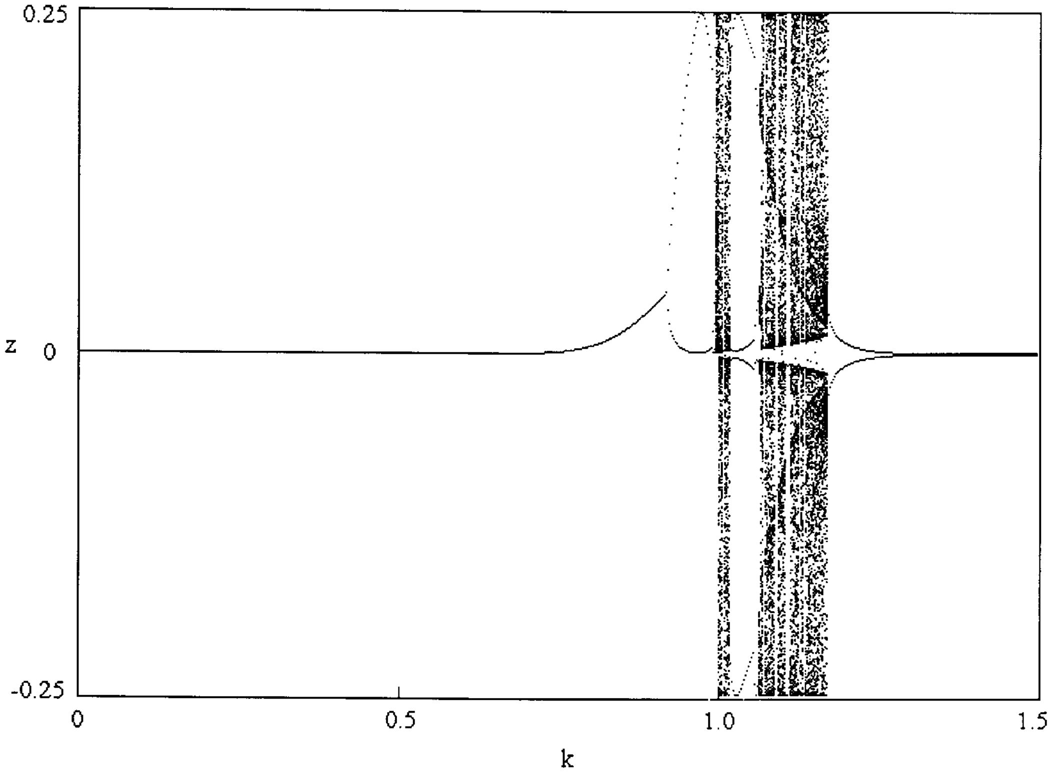

Figure 2.17: Bifurcation diagram for $k = k' \neq 1$ at $a = 50, b/a = 0.5$

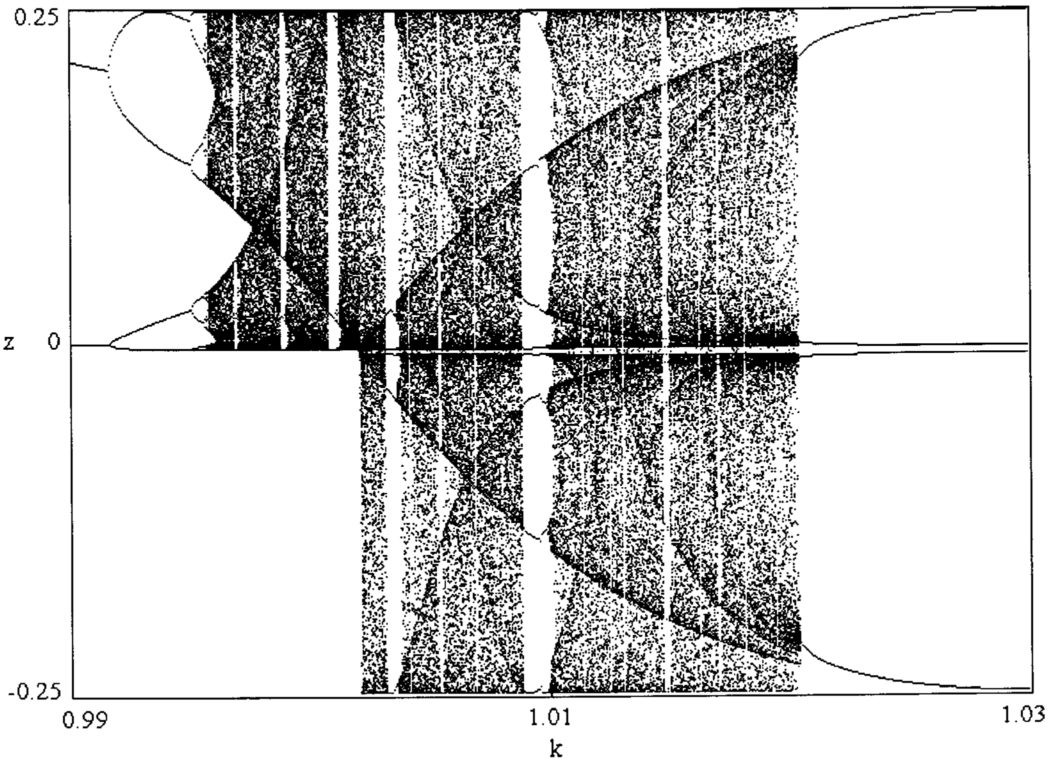

Figure 2.18: Magnified view of bifurcation diagram for $k = k' \neq 1$ at $a = 50, b/a = 0.5$ over the interval $0.99 \leq k \leq 1.03$

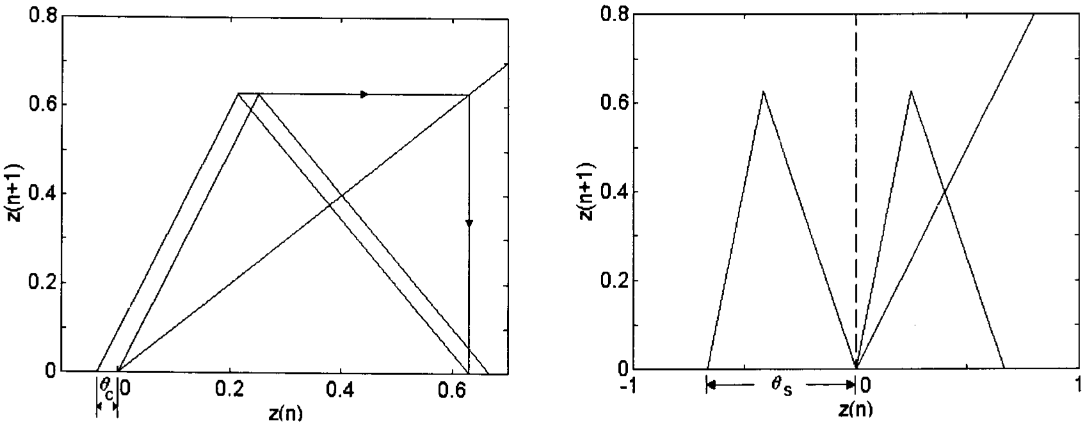

(a) (b)

Figure 2.19: (a) The critical bias (θ_c) and (b) the saturation bias (θ_s).

external input

$$Z_{n+1} = F_a(Z_n + \theta) - F_b(Z_n + \theta). \tag{2.20}$$

An identical equation is obtained if, instead of an external input, we had introduced a negative threshold (i.e., bias) of magnitude θ. In what is to follow, we will not therefore differentiate between bias/threshold and a constant amplitude external input. The effect of introducing a constant perturbation in simple chaotic maps, have been previously observed to give rise to 'non-universal' behavior (i.e., the nature of response differ from one map to another) [187, 175]

Let us first consider the case when $\theta > 0$ (we will refer to this as 'bias'). As θ increases from 0, the map shifts to the left, and the origin, $Z_1^* = 0$, is no longer a fixed point. Two values of θ are of interest in understanding what changes are made to the autonomous system dynamics by this modification.

- The *critical bias* (θ_c) is the bias value at which the critical point of the one-dimensional map (representing the dynamics of the system) is mapped to 0. This marks the transition point from chaotic behavior to superstable cycles (Fig. 2.19 (a)).
- The *saturation bias* (θ_s) is the bias value at which $Z_1^* = 0$ again becomes a fixed point, in fact, a stable one - i.e., for any initial value, Z_0, the trajectory terminates at $Z_1^* = 0$. This occurs when the entire non-zero portion of the map shifts to the left of the origin, so that the point $Z = 1/b$ in the original map, now coincides with the origin.

An expression for the critical bias is obtained, in the case of the asymmetric piecewise linear transfer function, by noting that for $\theta = \theta_c$, $F_a(\frac{1}{a} + \theta) - F_b(\frac{1}{a} + \theta) = 0$. So,

$$\theta_c = \frac{1}{b} + \frac{b}{a} - 1.$$

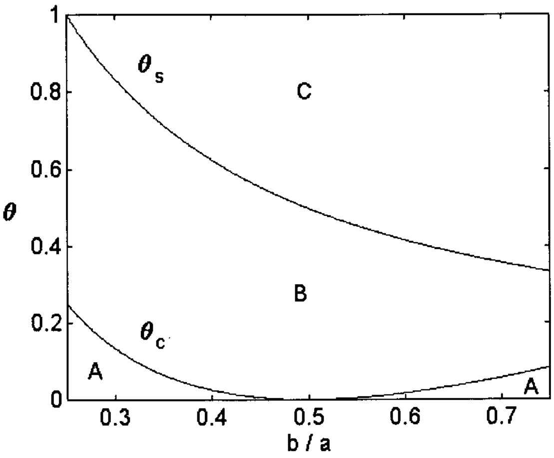

Figure 2.20: The μ vs θ parameter space indicating regions of (A) chaotic, (B) superstable period cycles and (C) fixed point ($Z^* = 0$) behavior, for $a = 4$.

The saturation bias, θ_s, is given as

$$\theta_s = 1/b.$$

These two expressions enable us to draw the (b/a) vs θ diagram in Fig. 2.20, showing the regions of different dynamical behavior.

When $\theta < 0$, coexistence of multiple attractors of different dynamical types is observed. Fig. 2.21 gives an example of the coexistence of a fixed point ($Z^* = 0$) and a chaotic attractor.

This allows the segmentation of activation state (X, Y)-space, according to dynamical behavior. For initial conditions lying in the region bounded by the two straight lines, $Y = (X - \theta)/k$ and $Y = (X - \theta)/(k - 1/ak)$, the trajectories are chaotic, provided the maximum point of the map, $F(Z) = 1 - (kb/a)$, does not iterate into the region $Z > \theta + (1/b)$. For the region, $Y > (X - \theta)/k$, any iterate will map to the fixed point, $Z^* = 0$. Initial conditions from $Y < (X - \theta)/(k - 1/ak)$ will map to the chaotic region, if the maximum point of the map does not iterate into $Z > \theta + (1/b)$. Otherwise, a fractal set of initial conditions will give rise to bounded chaotic motion, the remaining region falling in the "escape set", eventually leading to periodic orbits.

The condition for coexistence of multiple attractors, in the case of $k = k' = 1$, is obtained as follows. The one-dimensional map equivalent to the excitatory-inhibitory system now has an unstable fixed point at $Z_u = \frac{\theta(a-b)}{a-b-1}$. Note that $Z^* = 0$ will always be stable for any $\theta < 0$. For two attractors to exist, the critical point of this modified map should not belong to the basin of attraction of $Z^* = 0$, which can be written as:

$$F_a(1 - \frac{b}{a}) - F_b(1 - \frac{b}{a}) > Z_u.$$

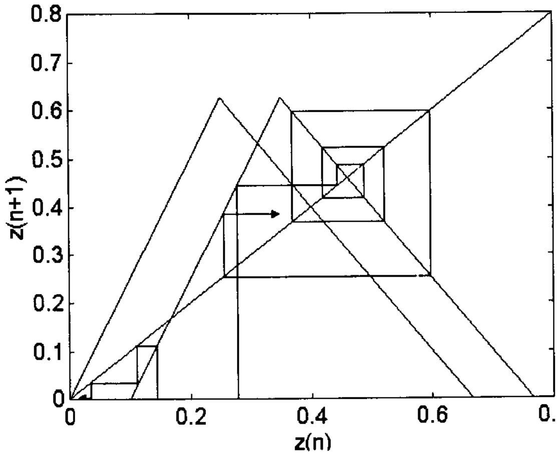

Figure 2.21: Coexistence of fixed point ($Z^* = 0$) and chaotic attractors, with trajectories in the two basins of attractions indicated, for $a = 4$, $b = 1.5$.

By simple algebraic manipulation, one obtains the following condition on the magnitude of θ:

$$\theta < \frac{(1 - b + \frac{b^2}{a})(a - b - 1)}{a - b - b(a - b - 1)}. \tag{2.21}$$

In the case of anti-symmetric activation functions, for a negative θ, $Z^* = 0$ is not a fixed point. Rather, under the condition mentioned above, the two disconnected chaotic attractors to be dynamically connected. This means, starting from an initial condition which belongs to one of the chaotic attractors, it is possible to visit the other attractor, provided the above condition is satisfied. This gives rise to hysteretic phenomenon in the model, as θ is monotonically increased or decreased.

Let us discuss the case of the anti-symmetric activation function given by Eqn. (2.10). As mentioned before, this has two coexisting chaotic attractors, in the two halves of the phase space: $L : (-\infty, 0)$ and $R : [0, \infty)$. In general, when $\theta > 0$, the trajectory remains in the attractor in R, whereas, if $\theta < 0$, it is confined to the attractor in L. Fig. 2.22 shows the bifurcations induced by varying θ, when the initial value, $Z_0 > 0$. It is apparent that the trajectory falls in the attractor in R, much before $\theta = 0$. On the other hand, for the initial value $Z_0 < 0$, a magnified view (Fig. 2.23) over the interval ($-0.01 < \theta < 0.01$), shows that the trajectory remains in L even after θ has become positive.

Simple hysteresis loops have been demonstrated and discussed by Harth (reviewed in [75] and the article by Harth in [6]) in neural populations containing mostly excitatory elements. Wilson and Cowan [204] showed that excitatory- inhibitory networks can show more complex hysteresis phenomena. For instance, multiple separated or simultaneous loops are observed, which is an outcome essentially of the inclusion of inhibition in the model.

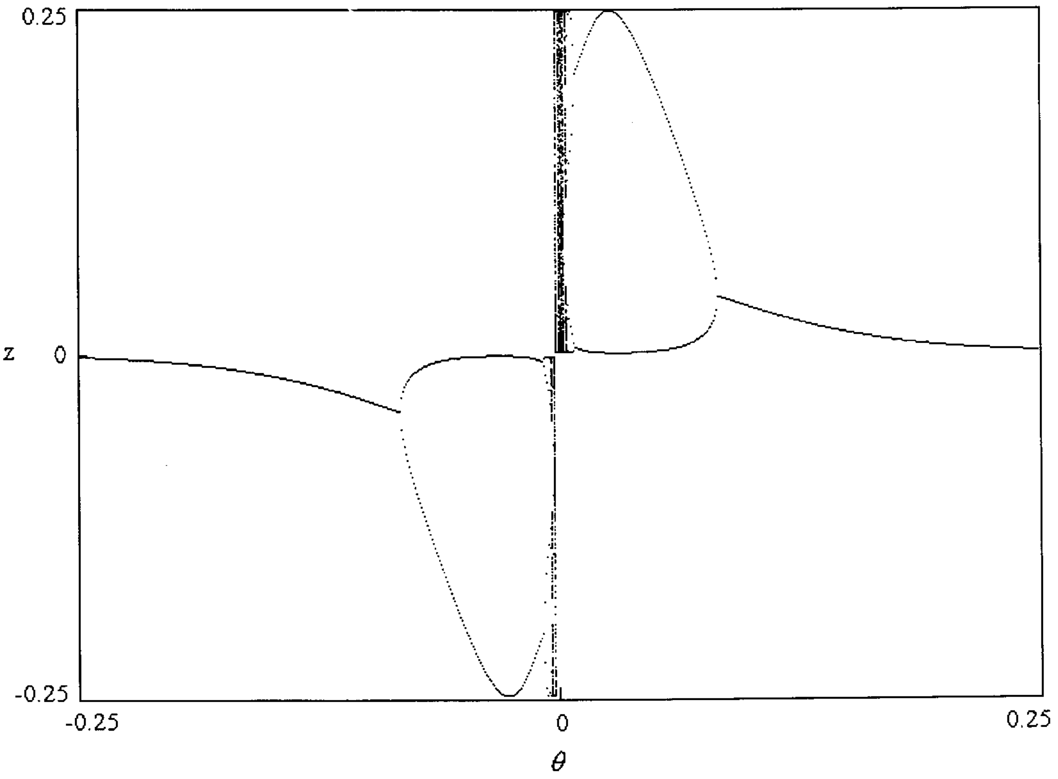

Figure 2.22: Bifurcation diagram for variation of threshold θ over the interval (-0.01, 0.01) for $a = 50, b/a = 0.5$ and $k = k' = 1$ (initial value, $Z_0 > 0$).

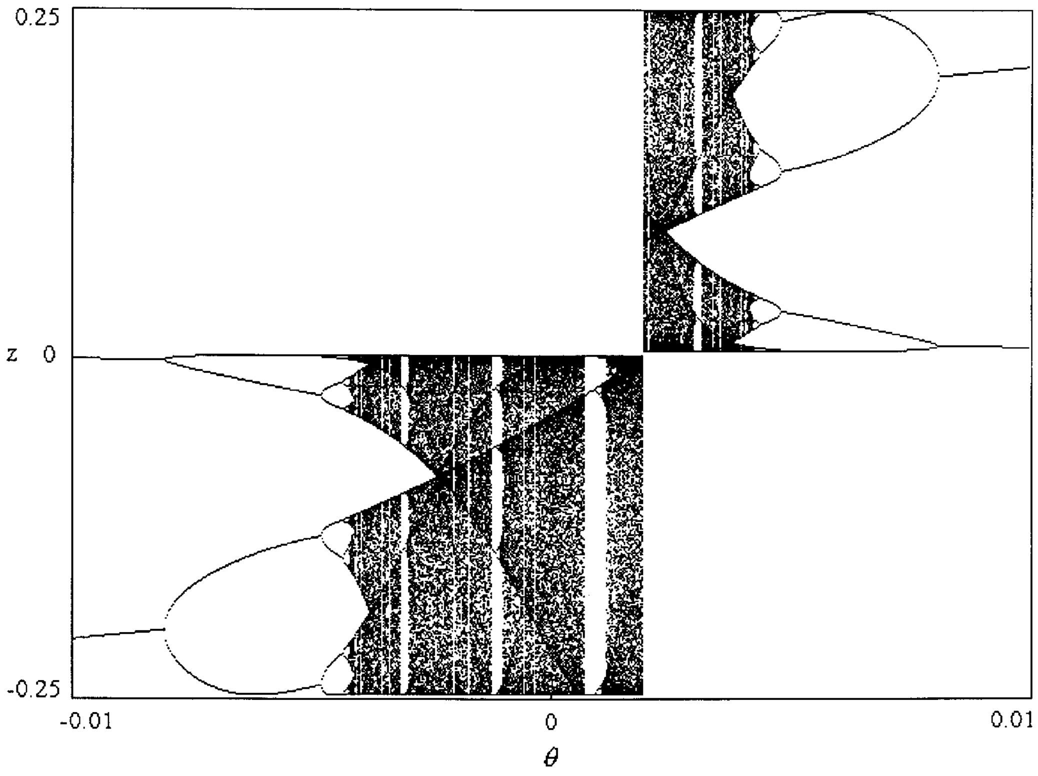

Figure 2.23: Magnified view of the bifurcation diagram for variation of θ over the interval (-0.25, 0.25) for $a = 50, b/a = 0.5$ and $k = k' = 1$ (initial value, $Z_0 < 0$).

Functionally, hysteresis may be a physiological basis for short-term memory. Any sufficiently strong stimulus is going to cause the activity to jump from a low level to a high level, and this activity will persist even after the input ceases. The existence of hysteresis in the central nervous system, specifically in the fusion of binocularly presented patterns to produce single vision, has also been experimentally verified. Hysteresis has the benefit of imparting robustness against noise. A large change in the external stimulus is needed to excite the element to a higher state, giving a threshold. For a complex system like the brain, that is immersed in a noisy environment, the advantage of such noise tolerance is obvious.

2.4 Extension to large networks

In the preceding sections, the behavior of a pair of excitatory-inhibitory neurons (number of neurons, $N = 2$) was shown to have sufficient complexity. The dynamics of a N-neuron network ($N >> 2$) described by

$$\mathbf{X_{n+1}} = F(\sum \mathbf{W}.\mathbf{X_n}),$$

where $\mathbf{X_n}$ is the set of N activation state values (both excitatory and inhibitory neurons), and $\mathbf{W}$ is the matrix of connection weights between different neurons. The full range of behavior shown by such a system will be impossible to study in detail, as the number of available tunable parameters are too large to handle. However, under certain restrictions, the dynamics of such large networks can be inferred.

Let W_{ij} denote the connection weight from jth to the ith neuron. Then, under the condition

$$W_{i\ j+1}/W_{i\ 1} = k_j, \quad (k_j = \text{constant for a given } j = 1, \ldots, N), \tag{2.22}$$

the N-neuron network dynamics is reducible to that of a 1-dimensional map with $(N+1)$ linear segments (for $\theta = 0$). The occurrence of "folds" in a map have already been shown to be responsible for creation and persistence of localized coherent structures within a chaotic flow [162]. As in this case, the resultant map will have a number of such folds, the system might show coexistence of multiple chaotic attractors (isolated from each other). A simple example to illustrate this point is a fully connected network of four neurons: two excitatory (x_1,x_2) and two inhibitory (y_1,y_2). Let a_i and b_i represent the slope of the transfer functions for the ith excitatory and inhibitory neurons, respectively. The 4-dimensional dynamics is reducible to the 1-dimensional dynamics of $z = x_1 - k_1 y_1 + k_2 x_2 - k_3 y_2$. Simulations were carried out for the set of parameter values: $(a_1 = 4.6, a_2 = 4.0, b_1 = 3.6, b_2 = 1.6)$ and $(k_1 = 0.7, k_2 = 1.0, k_3 = 1.1)$. Furthermore, x_2,y_2 have a threshold equal to $1/b_1$. Fig. 2.24 (a) shows the return map and time evolution of z in the absence of any bias. There is only a single global chaotic attractor in this case. When a small negative bias is applied to the whole network, the previous attractor splits into two coexisting

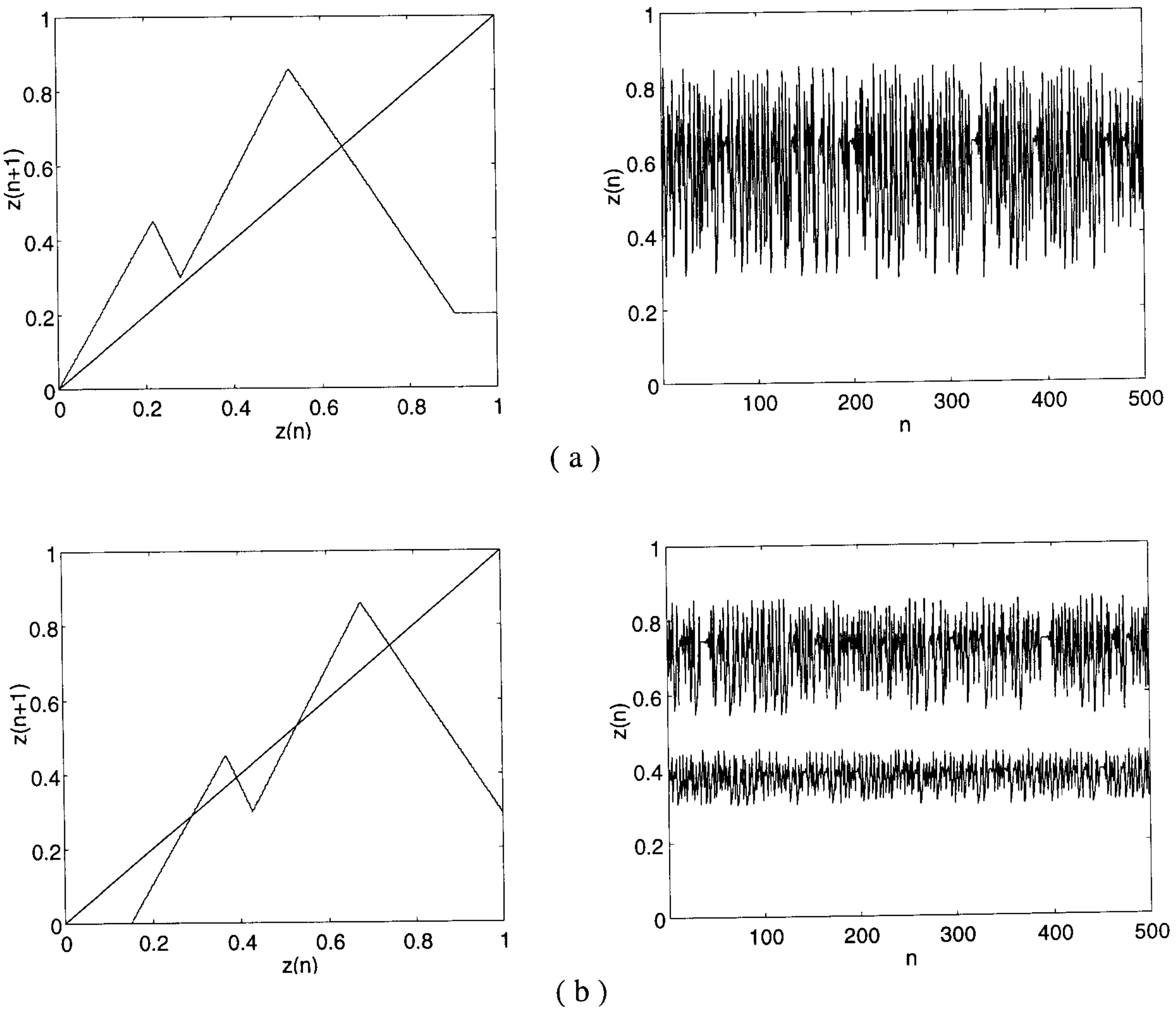

Figure 2.24: The return map and time evolution of the reduced variable, z, for a 4-neuron network (for details see text), with (a) bias = 0 and (b) bias = − 0.15. In the former there is a single global chaotic attractor. For non-zero bias, there are two co-existing chaotic attractors. Time evolution of z starting from two initial conditions belonging to different attractors are superposed.

isolated attractors having localized chaotic activity. Which attractor the system will be in, depends upon the initial value it starts from. Fig. 2.24 (b) shows the return map for a bias value of -0.15 and the superposed time evolutions of z starting from initial conditions belonging to two different attractors. So, an increase in bias, can cause transition from global chaos to localized chaotic regions.

This property can be used to simulate a proposed mechanism of olfactory information processing [53]. It has been suggested that the olfactory system maintains a global attractor with multiple "wings", each corresponding to a specific class of odorant. During each inhalation, the system moves from the central chaotic repeller to one of the wings, if the input contains a known stimulus. The continual shift from one wing to another via the central repelling zone has been termed as chaotic "itinerancy". This forms the basis of several chaotic associative memory models.

The above picture can be observed in the present model by noting that, if the external input has the effect of momentarily increasing the bias from a negative value to zero, then the isolated chaotic regions merge together into a single global attractor. In this condition, the entire region is accessible to any input state. However, as the bias goes back to a small negative value, the different isolated chaotic attractors re-emerge, and the system dynamics is constrained into one of these. Sustained external stimuli will cause the gain parameters to decrease (adaptation), thereby decreasing the local slope of the map. If the stimulus is maintained, the unstable fixed point in the isolated region will become stable leading to a fixed-point or periodic behavior. The above scenario, in fact, is the basis of using the proposed model as an associative memory network.

2.5 Information processing with chaos

Chaotic dynamics enables the microscopic sensory input received by the brain to control the macroscopic activity that constitutes its output. This occurs as a result of the selective sensitivity of chaotic systems to small fluctuations in the environment and their capacity for rapid state transitions. On the other hand, chaotic attractors are globally extremely robust. These properties indicate that the utilization of chaos by biological systems for information processing can indeed be advantageous. It has been suggested, based on investigations into cellular automata, that complex computational capabilities emerge at the "edge of chaos" [109].

Based on this notion, efforts are on to use chaos in neural network models to achieve human-like information processing capabilities. Chaotic neural networks have been already been applied in designing associative memory networks [96] and solving combinatorial optimization problems, using chaos to carry out an effective stochastic search [94]. The superposition of chaotic maps for information processing has also been suggested before [10, 9].

The model presented in this chapter can be used for a variety of purposes, classified as follows:

Associative memory: A set of patterns (i.e., specific network state configurations) are stored in the network as attractors of the system dynamics, such that, whenever a distorted version of one of the patterns is presented to the network as input, the original is retrieved upon iteration. The distortion has to be small enough so that the input pattern is not outside the basin of attraction of the desired attractor. In networks using convergent dynamics, the stored patterns necessarily have to be time-invariant or at most, periodic.

Chaos provides rapid and unbiased access to all attractors, any of which may be selected on presentation of a stimulus, depending upon the network state and external environment. It also acts as a "novelty detector", classifying a stimulus as being previously unknown, by not converging to any of the existing attractors. This suggests the use of chaotic networks for *auto association.*

In the previous section, the basic mechanism for constructing an associative memory network has been described. In this proposed model, both constant and periodic sequences can be stored. This is made possible by introducing "folds" in the return map of the network, so that a large number of isolated regions are produced. The nature of the dynamics in a region can be controlled by altering the gain parameters of individual neurons. Accessibility to a given attractor depends upon the initial condition of the network and the input stimulus. So, regions with fixed-point or periodic attractors may be embedded within regions having chaotic behavior. In addition, chaotic trajectories confined within a specific region can also be generated when presented with a short-duration input stimulus belonging to that region. "Novelty detection" is implemented in the above model by making the basins of attractors (corresponding to the stored patterns) of some pre-specified size. Input belonging outside the region, therefore, cannot enter the basin and will not be able to converge to the stored pattern.

Pattern classification: In this information processing task, different input sets need to be classified into a fixed number of categories. Decision boundaries, i.e., boundaries between the different classes are constructed by a "training session" where the network is presented with a series of inputs and the corresponding class to which they belong. In the proposed model, classification can be on the basis of dynamical behavior. For example, input sets belonging to different input classes may give rise to different periodic sequences. Otherwise, the distinction can be made between categories of inputs which give rise to chaotic and non-chaotic trajectories. For a pair of neurons ($N = 2$), under the condition $k = k'$, linear separation of the (X, Y)-space can be done (as shown above). By varying the parameters k and b the orientation and size of the class regions can be controlled. If $k \neq k'$ and $N > 2$, nonlinear decision boundaries between different classes can be generated. By using suitably adjusted weights, any arbitrary classification can be achieved.

An example of nonlinear decision boundary generation is shown in Fig. 2.25. The network used for this purpose consists of 4 neurons - 2 excitatory (x_1, x_2) and 2

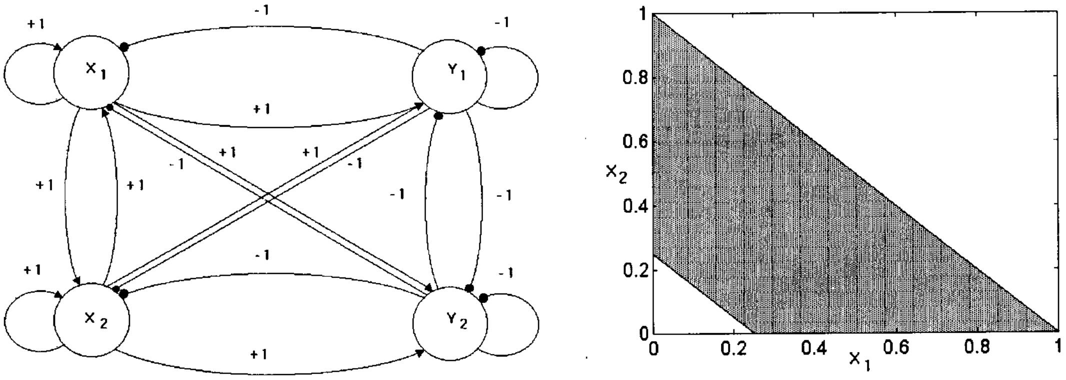

(a) (b)

Figure 2.25: (a) A fully connected 4-neuron network with 2 excitatory ($x_{1,2}$) and 2 inhibitory ($y_{1,2}$) neurons. The arrows and circles represent excitatory and inhibitory synapses, respectively. (b) The (x_1, x_2) phase space shows the basin of the chaotic attractor (shaded region) for threshold, θ=0.25. The unshaded region corresponds to fixed point behavior of the network.

inhibitory (y_1, y_2) (Fig. 2.25 (a)) with asymmetric, piecewise linear activation functions. The gain parameters are $a_{x_1,x_2} = 2$ and $b_{y_1,y_2} = 1$. All the neurons have a threshold, θ. The network is fully connected with all weightages equal to unity. The input stimulus is taken to be the initial value of the excitatory neurons and the inhibitory neuronal states are initially taken to be zero.

As shown in Fig. 2.25 (b), for $\theta = 0.25$, the (x_1, x_2) phase space is segmented into basins leading either to fixed point or to chaotic attractors. By increasing θ, the width of the chaotic band can be reduced. Changing the initial value of the inhibitory neurons will cause translation of the band and manipulating the connection weights gives a rotation to the band. Thus, any general transformation can be applied to the segment. More complex network connections might permit segmenting isolated box-like regions in the phase space. This possibility is currently under investigation.

System Dynamics Approximation: A system may be described by a nonlinear input-output relation,

$$Y = \mathbf{G}(X),$$

where the mapping function, $\mathbf{G}$, is unknown. By having access to a limited set of input-output pairs, the function has to be approximated - in effect, building a system simulator. Jin *et al* have proposed a discrete-time recurrent neural network [97], which is non-chaotic but similar to the present model, in order to approximate discrete-time systems [98]. In the present model, a sufficient number of coupled neurons can be used to construct any arbitrary piecewise linear input-output relation. By use of a suitable learning rule, the available data set can be used to determine the gain parameters, thresholds and connection weights of the network. A close approximation of the system dynamics will enable prediction and control of its behavior. The approximation's accuracy is not restricted to systems with piecewise linear functions - but can also give good qualitative reconstruction of smooth nonlinear systems.

Periodic sequence generation: Capability for periodic sequence generation can be exploited for modeling *central pattern generators.* These are a class of biological neural ensembles which control well-defined rhythmic muscle movements such as swimming, running, walking, breathing, etc. Usually they are found in the spinal cord, producing periodic sequences without feedback from the motor system or higher-level control. The ability to generate multiple sequences from the same neural assembly is another interesting feature. Postulating the existence of single pacemaker neurons acting as the 'system clock' to initiate periodic activity cannot explain all the observed phenomena. The existing network models for simulating this behavior mostly suffer from the drawback that they cannot generate multiple non-overlapping sequences. This shortcoming is overcome in the model presented here. For $N = 2$ and $k = k' \neq 1$, a rich variety of periodic sequences can be chosen from the same network, simply by altering the gain parameters by a very small amount. As mentioned above, numerical investigations indicate that cycles of any period can be generated by suitably altering the value of k.

2.6 Discussion

One notable feature of our investigations is the existence of the wide range of dynamical behavior in the simple system of a coupled neuron pair, which has been observed with a variety of nonlinear activation functions. In addition to the functions considered here, other types of nonlinear activation functions, e.g., $F_a(z) = tanh(z/a)$ and $F_a(z) = \frac{2}{\pi}\arctan(z/a)$ also show qualitatively similar features. In this context, it may be remarked that a related form of activation function: $F_a(z) = \frac{1}{1+\exp(-az)}$ has been shown to be topologically conjugate to the chaotic logistic map by Wang [197]. The universality of the observed dynamical features argue strongly that the observations reported here are not merely artifacts of the specific type of function chosen, but in fact, have a broader relevance.

As mentioned previously, we have not considered delayed interactions in our model. The introduction of delays in a neural system can produce qualitatively different behavior. Such effects have been observed in continuous-time [16] and discrete-time [116, 43] updated neural networks. A particularly simple form of delay, viz., an unbounded, exponentially decreasing delay is amenable to simple theoretical analysis [39]. Including this type of delayed interaction in our model shows no new qualitative features. However, other types of delay might produce new, interesting behaviors in the system.

To summarize, the behavior of an excitatory-inhibitory neural pair has been studied in detail for $N = 2$ (where N is the number of neurons). Nonetheless it shows capability for supporting extremely complex behavior. Under certain restrictions, the dynamics for $N >> 2$ networks can also be understood. Relaxation of these restrictions will provide a challenging task for the future.